



## Thermal and shape properties of asteroid (21) Lutetia from Herschel observations around the Rosetta flyby <sup>☆</sup>, <sup>☆</sup> <sup>☆</sup>

L. O'Rourke <sup>a,\*</sup>, T. Müller <sup>b</sup>, I. Valtchanov <sup>a</sup>, B. Altieri <sup>a</sup>, B.M. González-García <sup>c</sup>, B. Bhattacharya <sup>d</sup>, L. Jorda <sup>e</sup>, B. Carry <sup>a</sup>, M. Küppers <sup>a</sup>, O. Groussin <sup>e</sup>, K. Altwegg <sup>f</sup>, M.A. Barucci <sup>g</sup>, D. Bockelee-Morvan <sup>g</sup>, J. Crovisier <sup>g</sup>, E. Dotto <sup>h</sup>, P. Garcia-Lario <sup>a</sup>, M. Kidger <sup>a</sup>, A. Llorente <sup>a</sup>, R. Lorente <sup>a</sup>, A.P. Marston <sup>a</sup>, M. Sanchez Portal <sup>a</sup>, R. Schulz <sup>i</sup>, M. Sierra <sup>a</sup>, D. Teyssier <sup>a</sup>, R. Vavrek <sup>a</sup>

<sup>a</sup> ESAC (European Space Astronomy Centre), PO Box 78, 28691 Villanueva de la Cañada, Madrid, Spain

<sup>b</sup> Max-Planck Institut für Extraterrestrische Physik (MPE) Garching, Germany

<sup>c</sup> INSA at ESAC (European Space Astronomy Centre), E-28691 Villanueva de la Cañada, Madrid, Spain

<sup>d</sup> NHSC, IPAC, CA, USA

<sup>e</sup> Laboratoire d'Astrophysique de Marseille, Marseille, France

<sup>f</sup> Bern University, Switzerland

<sup>g</sup> LESIA, Observatoire de Paris, 5 Place Jules Janssen, 92195 Meudon, France

<sup>h</sup> INAF Osservatorio Astronomico di Roma

<sup>i</sup> ESA Research and Scientific Support Department, ESTEC, Noordwijk, Netherlands

### ARTICLE INFO

#### Article history:

Received 22 May 2011

Received in revised form

28 November 2011

Accepted 9 January 2012

Available online 24 January 2012

#### Keywords:

Lutetia

Herschel

Rosetta

Thermophysical modelling

TPM

Thermal Inertia

Albedo

H-mag

### ABSTRACT

Prior to and around the Rosetta flyby of (21) Lutetia, the Herschel Space Observatory performed a collaborative observation campaign with its two photometers observing the asteroid in the far infrared, at wavelengths not covered by Rosetta's instruments. The Herschel observations, fed into a thermophysical model (TPM) using as input a shape model based on in-situ images, were also further correlated with  $\sim 70$  multi-wavelength observations of Lutetia. We confirm the geometric albedo measured by Rosetta, derive a H-mag value based upon the effective diameter of the asteroid and point to (21) Lutetia having an extremely low thermal inertia ( $5 \text{ J m}^{-2} \text{ s}^{-0.5} \text{ K}^{-1}$ ). This thermal inertia is only possible through the existence of a significant amount of small scale roughness which is not directly observable by the OSIRIS (Optical, Spectroscopic, and Infrared Imaging System) instrument on-board Rosetta. In addition, our results point to the existence of a hill/crater surface feature located on the asteroids southern region not observed by Rosetta. From our results, we conclude that only through the merging of in situ and remote sensing observations can a true global picture be obtained of this asteroid.

© 2012 Elsevier Ltd. All rights reserved.

## 1. Introduction

Remote sensing and in-situ measurements are considered highly complementary in nature: remote sensing shows the global picture, but conversion of measured fluxes in physical quantities depends upon model assumptions to describe surface properties. In-situ techniques measure physical quantities in a more direct way e.g., size, shape, geometric albedo or surface

details. However, such techniques are often limited in spatial coverage (flybys) and results from disk-resolved observations are often not directly usable for the interpretation of global, disk-integrated properties e.g., local temperature versus thermal inertia.

Numerous studies have taken place of the peculiar (Barucci et al., 2008) asteroid (21) Lutetia based upon ground and space based observations. Once this asteroid was selected as a Rosetta flyby target, it became an important object to observe for two main reasons. First, it provided input to the Rosetta team as to the thermal and physical conditions existing on the asteroid. Secondly, it allowed the comparison of the pre-flyby measurements with those produced as output of the flyby with the associated benefits e.g., confirming the model accuracy that arises as a result. Such studies (see Table 1) have provided estimates of optical and thermal properties for this asteroid (geometric albedo, inertia)

<sup>\*</sup> Herschel is an ESA space observatory with science instruments provided by European-led Principal Investigator consortia and with important participation from NASA.

<sup>☆</sup> Analysis is also based on observations collected at the European Southern Observatory, Chile; ESO, No. 79.C-0006.

<sup>\*</sup> Corresponding author. Tel.: +34 918 131 363.

E-mail address: [lorourke@esa.int](mailto:lorourke@esa.int) (L. O'Rourke).

**Table 1**  
Summary of thermal and physical properties of (21) Lutetia.

Geometric Albedo ( $p_V$ )	Thermal inertia $Jm^{-2} s^{-0.5} K^{-1}$	Beaming factor ( $\eta$ )	Effective diameter (Deff – km)	G (mag)	H (mag)	Roughness ( $\rho, f$ )	Reference
$0.2212 \pm 0.020$		0.756	$95.76 \pm 4.1$	0.11	7.35		Tedesco, 1992
$0.208 \pm 0.025$	< 50	0.93/0.94	$98.3 \pm 5.9$	0.11	7.35		Tedesco et al., 2001
0.1							Mueller et al., 2006
$0.129 + 0.003 - 0.03$	5.2						Zellner and Gradie, 1976
			~110				Carvano et al., 2008
$0.18^a - 0.22^b$				0.125	7.25		Drummand et al., 2009
$0.13$ and $0.26^c$	$\leq 30$	~0.70–0.83					Belskaya et al., 2010
							Lamy et al., 2010
0.19			$98 \pm 2$				Sierks et al., 2011
$0.20 \pm 0.01$	< 10		95.97	0.12		$\rho=0.6$ $f=0.7$	Present Study
	Best fit 5						

<sup>a</sup>  $p_V$  based on Deff from Drummand et al., 2009.

<sup>b</sup>  $p_V$  based on Deff from Mueller et al., 2006.

<sup>c</sup>  $p_V$  from Mueller et al., 2006, where  $p_V$ =geometric albedo, Deff=effective diameter.

which served as important inputs when preparing for in-situ based observations.

These inputs could be verified by in-situ/flyby observations which provide the “ground truth” for the asteroid, however such a comparison is limited in nature and it is only through the execution of a combined observation campaign with both remote and in-situ/flyby data at similar epochs that the final calculated properties can be obtained. The output of such an observation campaign can be maximised if the observations are taken with similar viewing conditions and if the flyby geometry visible to the in-situ spacecraft is matched to that from the remote spacecraft observations thus comparing, from an observation perspective, like with like. Additionally, having instruments on both spacecraft complementing one another through looking at the object at similar wavelengths serves to reinforce the science results generated from both. With such approaches being applied, one can obtain highly accurate values for surface composition, reflectance, thermal inertia and temperatures, thus greatly improving the scientific understanding of the object in question.

Indeed, these are the properties which provide confidence not only in the accuracy of the pre-flyby results but also in the techniques used as input in deriving those results, especially where it is clear that not all asteroids can have the benefit of an in-situ observation campaign. As a minimum, by confirming the validity of such remote based measurement techniques, one can apply them to objects of a similar size and makeup.

The above approaches were followed with the Herschel Space Observatory SPIRE (Spectral and Photometric Imaging Receiver, Griffin et al., 2010) instrument observing (21) Lutetia less than 1 day after the Rosetta flyby in a similar viewing epoch as seen by Rosetta instruments. Measurements taken at the end of 2009 and approximately 24 day before the flyby by the PACS (Photodetector Array Camera and Spectrometer, Poglitsch et al., 2010) instrument helped to reinforce those results and indeed contribute to the extraction of the thermal inertia, surface roughness, shape model discrepancies and measured surface temperature. We compare our results not only with the Rosetta MIRO and VIRTIS (Visible and Infrared Thermal Imaging Spectrometer) instrument flyby measurements (whose wavelength ranges are highly complementary to those of Herschel PACS and SPIRE) but also utilise data from other observatories (Spitzer, ESO-VISIR, Akari) in our analysis to complete the quite significant data set of 92 observations in use in this current study.

In this paper, we firstly present the PACS and SPIRE observations taken of (21) Lutetia, the data reduction, and the results obtained. We follow this with the measurements derived from

other observatories to feed into our thermal model. We proceed to introduce the shape model and the thermal model we have used to analyze the above results, followed by a description of the  $H$ - $G$  values and the albedo calculated by us and confirmed through direct measurements by Rosetta at the asteroid. We then derive the thermal inertia for a range of different surface roughness levels. At this point we present the impact of our results on the shape model in use and identify shortcomings and necessary modifications in this shape model (beyond the Rosetta results). We finally conclude the paper with the implications of our results on current and future asteroid research.

## 2. Observations with the Herschel space observatory

### 2.1. Observations of (21) Lutetia with the PACS & SPIRE instruments

The European Space Agency's (ESA) Herschel Space Observatory (Pilbratt et al., 2010), launched in 2009, performs observations from the 2nd Lagrangian point ( $L_2$ ) at  $1.5 \times 10^6$  km from Earth. It has three science instruments on board covering the far-infrared part of the spectrum, two of which, PACS and SPIRE, have been used to observe (21) Lutetia.

Although covering different wavelengths from those of the Rosetta instruments, the wavelength ranges of the PACS and SPIRE photometer instruments were found to match extremely well however with the Rosetta MIRO and VIRTIS instruments i.e., PACS 60–210  $\mu m$  versus VIRTIS ending at 5  $\mu m$ , SPIRE 250–500  $\mu m$  versus MIRO starting at 530  $\mu m$ .

In advance of the flyby, two observation data sets for PACS (2009-Dec-21 and 2010-June-17, See Table 2 and Fig. 1 PACS Image) already existed for this asteroid, however no SPIRE data had yet been taken. In this respect, a dedicated campaign was organized around the flyby to further obtain SPIRE measurements and as a result complete the full data set from Herschel of this asteroid.

The SPIRE photometer imaged the asteroid on the 2010-July-11 at a time exactly 2 rotation periods (16.34 h) after the flyby. The SPIRE observation (Table 2, Fig. 1 SPIRE image) was timed to be as close as possible to the asteroid visibility conditions observed by Rosetta instruments in its flyby.

### 2.2. Data reduction and results from the SPIRE observations

The SPIRE observations were processed with the SPIRE Photometer pipeline version 5.0 in the Herschel Interactive Processing

**Table 2**  
SPIRE and PACS instrument measurements — observation details. OBSID=observation identifier. The phase angle is negative for those observations taken after opposition and positive for those taken before opposition.

Instr.	epoch (UT, date/start time)	OBSID	Wavelength ( $\mu\text{m}$ )	Instrument observing mode	helio-centric distance ( $r$ — AU)	Herschel-centric distance ( $l$ — AU)	phase angle ( $\alpha$ — $^\circ$ )
SPIRE	2010-07-11T07:55:55	1342,200,204	250/350/500	Cross_scan	2.719	3.054	−19.37
PACS	2009-12-21T01:43:41	1342,188,332	100/160	chop-nod	2.833	2.507	20.31
PACS	2009-12-21T01:47:26	1342,188,333	70/160	chop-nod	2.833	2.507	20.31
PACS	2009-12-21T01:51:11	1342,188,334	100/160	scan-map	2.833	2.507	20.31
PACS	2009-12-21T01:56:28	1342,188,335	100/160	scan-map	2.833	2.507	20.31
PACS	2009-12-21T02:01:45	1342,188,336	100/160	scan-map	2.833	2.507	20.31
PACS	2009-12-21T02:07:02	1342,188,337	100/160	scan-map	2.833	2.507	20.31
PACS	2010-06-17T17:05:26	1342,198,492	100/160	scan-map	2.744	2.785	−21.39
PACS	2010-06-17T17:11:15	1342,198,493	100/160	scan-map	2.744	2.785	−21.39
PACS	2010-06-17T17:17:04	1342,198,494	70/160	scan-map	2.744	2.785	−21.39
PACS	2010-06-17T17:22:53	1342,198,495	70/160	scan-map	2.744	2.785	−21.39

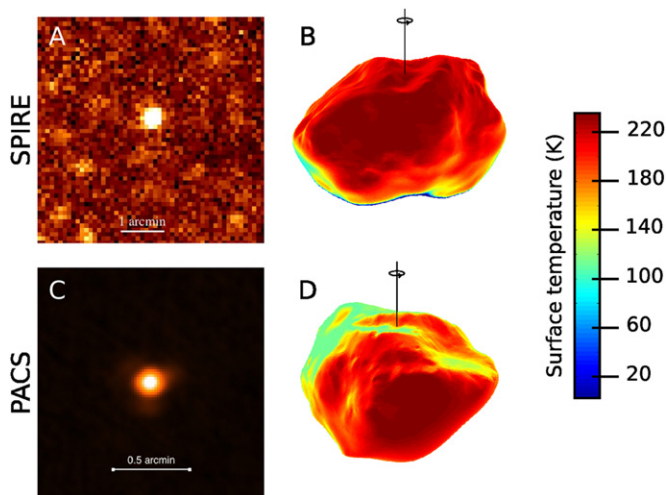


**Fig. 1.** (A) SPIRE (2010-July-11) 250  $\mu\text{m}$  image with background galaxies visible (B) Observing geometry and TPM apparent temperature map at same epoch consistent with Rosetta flyby viewing geometry. (C) PACS (2009-Dec-21) 100  $\mu\text{m}$  image — the 3 lobes correspond to the structured PSF (D) Observing geometry and TPM apparent temperature map on that date. For both B and D, the representation of Lutetia is colour coded according to surface temperature. The surface temperature is calculated using default parameters for roughness and emissivity (Mueller & Lagerros 2002) combined with the derived thermal inertia from this paper of 5 SI.

Environment (HIPE,<sup>1</sup> Ott et al., 2009). The latest SPIRE calibration files were used with flux calibration based on Neptune. Lutetia was clearly seen in the three SPIRE maps at 250, 350 and 500  $\mu\text{m}$  as a unresolved, point-like source. To derive the flux densities, a 2-D circular Gaussian was fitted to the timeline data of the SPIRE detectors. The derived monochromatic flux densities were then colour corrected for a source with a spectral shape proportional to  $\nu^2$  (the standard SPIRE Photometer pipeline gives the monochromatic flux densities for a source with a spectral shape  $\sim 1/\nu$ ). The final flux density errors include a 7% conservative flux uncertainty from the Neptune model, in addition to the fitted peak error.

The fluxes corresponding to the three SPIRE wavelength bands and associated errors are provided in Table 3 whereby the following FWHM (Full Width Half Maximum) were fixed for the relevant wavelengths (250/350/500  $\mu\text{m}$ ), respectively: 17.6"/23.9"/35.1"

<sup>1</sup> HIPE is a joint development (are joint developments) by the Herschel Science Ground Segment Consortium, consisting of ESA, the NASA Herschel Science Centre, and the HIFI, PACS and SPIRE consortia.

### 2.3. Data reduction and results from the PACS observations

The PACS measurements were processed using HIPE 5.0 (Ott et al., 2009). The derived fluxes were aperture and colour corrected to obtain monochromatic flux densities at the PACS reference wavelengths. The colour correction values for (21) Lutetia of 1.00, 1.02, 1.05 in blue (70  $\mu\text{m}$ ), green (100  $\mu\text{m}$ ) and red (160  $\mu\text{m}$ ) bands are based on a thermophysical model SED (Spectral Energy Distribution), corresponding roughly to a 200 K black-body curve. The flux calibration was verified by a set of 5 high-quality fiducial stars ( $\beta$  And,  $\alpha$  Cet,  $\alpha$  Tau,  $\alpha$  Boo and  $\gamma$  Dra, which have been observed multiple times in both of the PACS observing modes used for our observations. Based on the analysis of the fiducial star measurements we adjusted the final Lutetia fluxes (average and stddev of all fiducial star observations divided by the corresponding model predictions). The final values obtained for the PACS instrument data sets were deemed to be accurate within 5% based upon existing calibrations.

The fluxes corresponding to the three PACS wavelength bands (70/100/160  $\mu\text{m}$ ) and associated errors are provided in Table 3.

### 3. Observations of (21) Lutetia with other observatories

To complete the data set which contains the previously presented measurements from the Herschel instruments, we also utilised data from other observatories. These are presented in Table 4 with references provided for those data sets which have been published. Reference is made to this current work for not only the Herschel unpublished data sets but also unpublished data from the ESO-VISIR and Spitzer-IRAC observatories.

Table 4 presents the list of observations covering the wavelengths from 7.8 to 500  $\mu\text{m}$ , phase angle from  $-29^\circ$  to  $+29^\circ$  and a rotational phase from  $3^\circ$  to  $358^\circ$ . The importance of this data set becomes clear in the coming section where such a comprehensive picture derived from the above parameters are key to extracting the main thermal parameters output from our thermal model.

#### 3.1. Observations of (21) Lutetia with ESO-VISIR

In 2004 we obtained ground-based N- and Q-band observations with the ESO-VISIR instrument (Lagage et al. 2004) mounted on the 8.2 m VLT telescope MELIPAL (UT 3) on Paranal.

This programme was optimised for the highest possible photometric accuracy and about half of the available observing time was spent on the monitoring of nearby calibration standards. The integration times per filter were between 60 and 90 s. A standard chopping and nodding technique was utilised for all observations

**Table 3**  
Derived flux densities — SPIRE (250,350,500  $\mu\text{m}$ ) & PACS (70/100/160  $\mu\text{m}$ ).

Instrument	Wavelength ( $\mu\text{m}$ )	OBSID	epoch (UT, date/start time)	Flux density (Jy)
SPIRE	250	1342,200,204	2010-07-11T07:55:55	$0.281 \pm 0.020$
SPIRE	350	1342,200,204	2010-07-11T07:55:55	$0.144 \pm 0.011$
SPIRE	500	1342,200,204	2010-07-11T07:55:55	$0.073 \pm 0.008$
PACS	70	1342,188,333	2009-12-21T01:47:26	$3.217 \pm 0.102$
PACS	70	1342,198,494	2010-06-17T17:17:04	$2.568 \pm 0.077$
PACS	70	1342,198,495	2010-06-17T17:22:53	$2.361 \pm 0.071$
PACS	70	1342,198,494+495 Combined		$2.48 \pm 0.074$
PACS	100	1342,188,332	2009-12-21T01:43:41	$1.788 \pm 0.058$
PACS	100	1342,188,334	2009-12-21T01:51:11	$1.816 \pm 0.055$
PACS	100	1342,188,335	2009-12-21T01:56:28	$1.819 \pm 0.055$
PACS	100	1342,188,334+335 Combined		$1.818 \pm 0.055$
PACS	100	1342,188,336	2009-12-21T02:01:45	$1.836 \pm 0.055$
PACS	100	1342,188,337	2009-12-21T02:07:02	$1.836 \pm 0.055$
PACS	100	1342,188,336+337 Combined		$1.837 \pm 0.055$
PACS	100	1342,198,492	2010-06-17T17:05:26	$1.587 \pm 0.048$
PACS	100	1342,198,493	2010-06-17T17:11:15	$1.532 \pm 0.046$
PACS	100	1342,198,492+493 Combined		$1.56 \pm 0.047$
PACS	160	1342,188,332	2009-12-21T01:43:41	$0.765 \pm 0.069$
PACS	160	1342,188,333	2009-12-21T01:47:26	$0.787 \pm 0.066$
PACS	160	1342,188,334	2009-12-21T01:51:11	$0.767 \pm 0.039$
PACS	160	1342,188,335	2009-12-21T01:56:28	$0.791 \pm 0.04$
PACS	160	1342,188,334+335 Combined		$0.781 \pm 0.039$
PACS	160	1342,188,336	2009-12-21T02:01:45	$0.816 \pm 0.041$
PACS	160	1342,188,337	2009-12-21T02:07:02	$0.809 \pm 0.041$
PACS	160	1342,188,336+337 Combined		$0.808 \pm 0.041$
PACS	160	1342,198,492	2010-06-17T17:05:26	$0.684 \pm 0.035$
PACS	160	1342,198,493	2010-06-17T17:11:15	$0.678 \pm 0.034$
PACS	160	1342,198,492+493 Combined		$0.682 \pm 0.034$
PACS	160	134,219,8494	2010-06-17T17:17:04	$0.644 \pm 0.034$
PACS	160	1342,198,495	2010-06-17T17:22:53	$0.633 \pm 0.032$
PACS	160	1342,198,494+495 Combined		$0.638 \pm 0.032$

to reduce the atmospheric and telescope background emission. Chop and nod throws were 8" respectively, the pixel scale was 0.07", the chopping frequency was 0.25 Hz (for filters PAH1, SIV, NeII) and 0.5 Hz (Q2). The corresponding central wavelengths are 8.59, 10.49, 12.81 and 18.72  $\mu\text{m}$ .

The final flux densities were determined via aperture photometry, the flux-conversion factors and air-mass corrections were established via the standard stars taken close in time. Overall, the observing conditions were very stable, resulting in small variations of the conversion factors. All stars and Lutetia were observed in a very reproducible way and the four chopped-nodded images were always located on exactly the same pixels on the array. Flat-field corrections were therefore not necessary.

For the calculation of the colour-correction terms (between stellar and Lutetia SEDs) we considered the full atmosphere and bandpass transmission profiles, resulting in corrections of 1–2%, depending on the band. The final error calculations included the error estimates for the conversion factor, the stellar models, the colour correction, the airmass correction, and the aperture photometry itself.

### 3.2. Observations of (21) Lutetia with Spitzer-IRAC

The NASA Spitzer Space Telescope was launched into an Earth-trailing orbit on August 25, 2003. The three instruments on board are capable of providing images and spectra from 3.6 to 160  $\mu\text{m}$  to sensitivities as low as a few Jy (Werner et al., 2004). As a part of the Infrared Array Camera (Fazio et al., 2004) (IRAC) Guaranteed Time Programme, asteroid (21) Lutetia was observed over a rotation period, in October 2007 and again in October 2008.

Thermal constraints required the observatory to look at targets with solar elongations in the range = 80°–120°. IRAC's pixel scale was 1.22"/pixel. The Spitzer observations are publicly available through the archive leopard interface <http://ssc.spitzer.caltech.edu/propkit/spot/> by querying for programme ID 30252. Raw, unprocessed individual frames as well as software pipeline-generated products are available. The pipeline provides background subtracted, flat-fielded, flux calibrated frames. For the IRAC data, we have worked with the Basic Calibrated Data (BCD) frames rather than mosaics. The final fluxes have been colour-corrected.

edu/propkit/spot/ by querying for programme ID 30252. Raw, unprocessed individual frames as well as software pipeline-generated products are available. The pipeline provides background subtracted, flat-fielded, flux calibrated frames. For the IRAC data, we have worked with the Basic Calibrated Data (BCD) frames rather than mosaics. The final fluxes have been colour-corrected.

## 4. Analysis of the thermal data

### 4.1. Shape and thermal model used

The analysis of the complementary measurements from both the Herschel and Rosetta spacecraft started with the inclusion into the TPM of the most up to date shape model (Jorda et al., 2010, 2011) of Lutetia existing at that time. This shape model was created based upon the Rosetta OSIRIS Instrument flyby data (disc resolved images) and remote sensing observations (lightcurves and disc resolved images (Carry et al., 2010; Drummond et al., 2009)). The shape model is referred to in the rest of the paper as the LAM (Laboratoire D'Astrophysique de Marseille) model.

The model has an effective size (of an equal volume sphere) of 98 km consisting of 45778 surface elements and 22891 vertices. It has a direction of the spin axis defined as: R.A. = 51.8°, DEC = +10.8°. This direction was derived directly from the flyby images. The spin rate was measured from ground-based data and is equal to  $8.16827043 \pm 0.00000001$  h. This low-resolution model has a mean horizontal resolution of 800 m and a vertical accuracy of about 20 m for the regions observed by OSIRIS measurements (about 60% of the surface) implying that the slopes are defined with an accuracy of about 1.5°. The accuracy is 5% in radius (about 3 km) for the regions constrained by remote sensing observations only (southern latitudes).

**Table 4**  
Details of all observations input into the model.

Instrument	No. of observations	Epoch	Phase ( $\alpha$ , deg.)	Rot. Phase ( $\phi$ , deg.)	Aspect ( $\theta$ , deg.)	Wavelength ( $\mu\text{m}$ )	References
SPIRE	3	2010-Jul-11	-19.4	267.8	118	250/350/500	This paper
PACS	16	2009-Dec-21	20.3	169.4, 176.0, 183.7	118.1	70/100/160	This paper
PACS	12	2010-Jun-17	-21.4	127.6, 136.1	111.2	70/100/160	This paper
IRAS	12	1983-Apr-25/26	-20.8	270.6, 5.2, 80.7	74.3/74.7	12/25/60/100	Tedesco et al., 2002
IRAS	8	1983-May-03/04	-20.8	108.9, 203.0	75.8/76.3	12/25/60/100	Tedesco et al., 2002
ESO-VISIR	15	2004-Oct-25	4.9	24.0...196.2	10.6	$3 \times (8.7, 10.38, 11.66, 12.35, 17.72)$	This paper
IRTF	3	2004-Jun-24	27.3	352.9, 358.1, 4.0	28.4	$1 \times (8.70, 11.60, 18.40)$	Mueller et al., 2006
Akari-IRC	5	2006-May-13/14	-21	229.1, 4.6, 305.6, 18.3, 91.1	90.6/91.0	$2 \times (9, 18); 1 \times 18$	This paper and Usui et al., submitted for publication <sup>a</sup>
Akari-IRC	6	2007-Feb-26/27	23.5	268.3, 341.3, 117.6, 190.6, 263.5, 336.5	163.1	$2 \times 9, 18; 2 \times 18$	This paper and Usui et al., submitted for publication <sup>a</sup>
ESO-TIMM2	3	2006-Jan-10	14.1	92.3, 101.9, 107.8	102.4	$1 \times (8.70, 10.35, 12.35)$	Carvano et al., 2008
Spitzer-IRAC-1C1	12	2007-Oct-17	-29.1	329.3 ... 300.7	147.1	$12 \times (7.87)$	This paper
Spitzer-IRAC-1C2	12	2008-Oct-31	25.4	335.0 ... 304.6	34.3	$12 \times (7.87)$	This paper

<sup>a</sup> Permission received from author to use the unpublished data.

The LAM shape model was imported into our Thermophysical model (TPM) (Lagerros, 1996, 1997, 1998). The TPM produces accurate thermal IR spectra and thermal light curves, taking into account a number of physical and thermal processes. In the TPM, the object is described by a given size, shape, spin state and albedo placed at the true observing and illumination geometry. The TPM considers a 1-D heat conduction into the surface and very importantly allows surface roughness to be included, described by “ $f$ ”, the fraction of the surface covered by spherical crater segments and “ $\rho$ ”, the rms of the surface slopes, connected to the crater depth.

The contributions of the subsurface emission at longer wavelength is accounted for by a wavelength-dependent emissivity decreasing from 0.9 at mid-IR (5 to 40  $\mu\text{m}$ ) to about 0.8 in the SPIRE range, derived from a combined set of large main-belt asteroids (Müller and Lagerros, 1998, 2002).

#### 4.2. Deriving the albedo & the “true” H-mag values

For the full treatment of the energy balance on each surface facet within the model, we need to describe the amount of reflected light. Our model is used regularly as a source for deriving asteroid size and albedo (Müller et al., 2005, 2011). The geometric visual albedo is derived taking into account the lightcurve averaged cross-sections for all observations which were used to calculate its absolute (optical) magnitude in the HG-system (Bowell et al., 1988). The values we use for  $G$  (slope parameter) and  $H$  (absolute magnitude) were obtained by Belskaya et al. (2010) are  $G=0.12$  mag and the  $H=7.25 \pm 0.01$  mag.

Using these values, we generate the geometric visual albedo  $p_V$  via the relation:

$$p_V = 10^{(6.2559 - 2 \times \text{ALOG}10(\text{Deff}) - 0.4 \times \text{Hmag})}$$

where 6.2559 is derived from the  $V$  — magnitude of the Sun of -26.74 mag (<http://nssdc.gsfc.nasa.gov/planetary/factsheet/sunfact.html>) at 1.0 AU.

The combination of the LAM shape model with the Belskaya et al. (2010) Hmag value leads to a  $p_V$  of  $0.20 \pm 0.01$ , which is in excellent agreement with the measured value from OSIRIS at zero phase angle of  $p_V=0.19$  (Sierks et al., 2011).

However, in our work to calculate the above  $p_V$  we identified an important factor behind the  $p_V$  value derivation which impacts significantly on the Hmag observed not only for Lutetia but also for other asteroids where shape models exist. This factor relates to the observable cross-section of the asteroid at the time of the observations in question. If one looks at the above Belskaya et al. (2010) value, it should be noted that these values were obtained from observations taken of the asteroid at aspect angles (connected to the true spin-axis) between  $160^\circ$  and  $175^\circ$  when the apparent cross-section of (21) Lutetia was approximately  $110 \text{ km}^2$ . To obtain the “true” Hmag, one must utilise observations taken at all aspect angles.

Based upon the LAM model which contains the true effective diameter of the asteroid (based upon flyby data), one can see that the above value of  $110 \text{ km}^2$  is much higher than the effective diameter of  $95.97 \text{ km}^2$ . The Hmag calculations are therefore constrained by the aspect angles visible at the time of the observations, and, if one is observing the asteroid at an aspect angle where the cross-section is much greater than its nominal effective diameter, then the final Hmag calculation is impacted. Knowing the shape model with an absolute size scale and the geometric albedo, one can determine a H-mag applicable for “all” aspect angles. Such a H-mag can then be considered as a general, object-specific property rather than an observed quantity which is only valid for certain aspect angles.

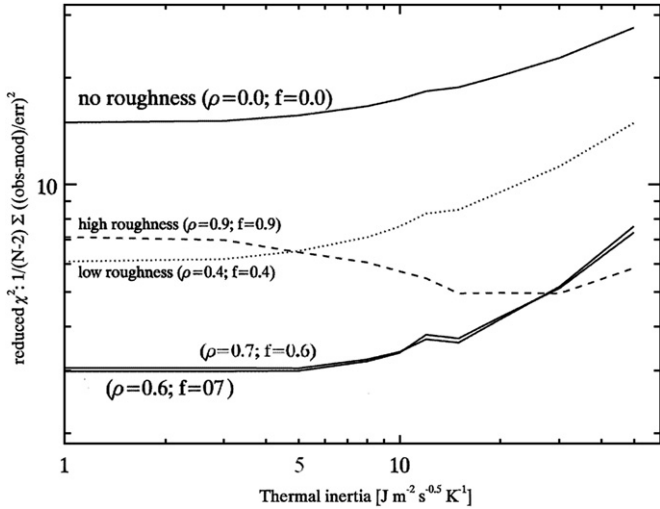


**Fig. 2.** Thermal Inertia  $\chi^2$  test — this figure shows the impact of roughness on the overall thermal inertia whereby the best fit lies clearly with roughness of  $\rho=0.6$  and  $f=0.7$ . The slope of this bottom curve can be seen to clearly rise after a thermal inertia of  $5 \text{ J m}^{-2} \text{ s}^{-0.5} \text{ K}^{-1}$  which allows us to conclude on this value as being the actual thermal inertia of (21) Luteta.

As a result, using the LAM model, the “true” H-mag for Lutetia, based upon the shape model with an effective diameter (of an equal volume sphere) of 95.97 km and an albedo of  $0.20 \pm 0.01$ , is calculated to be  $H\text{-mag} = 7.48 \pm 0.03$ .

These two values were fed into the radiometric analysis described in the next subsection via the TPM code to us to derive a conclusive value for the surface roughness and thermal inertia of (21) Lutetia.

### 4.3. Surface roughness and thermal inertia of (21) Lutetia

As described in Sections 2 and 3, 92 observations from different observatories were fed into the model. The thermal model was therefore run not only against Herschel PACS and SPIRE observations, the key data set for this analysis, but also a comprehensive set of 76 observations made of Lutetia by other observatories as described in Table 4.

A TPM  $\chi^2$  test was run using a range of thermal inertias (from 1 to 50) with the goal to find the best fit obtained with a specific thermal inertia value when comparing the observation/TPM ratio with phase angles, wavelength, rotational phase and aspect angle.

The initial result of this  $\chi^2$  test showed that a driving constraint on all parameters was the surface roughness. The analysis of the

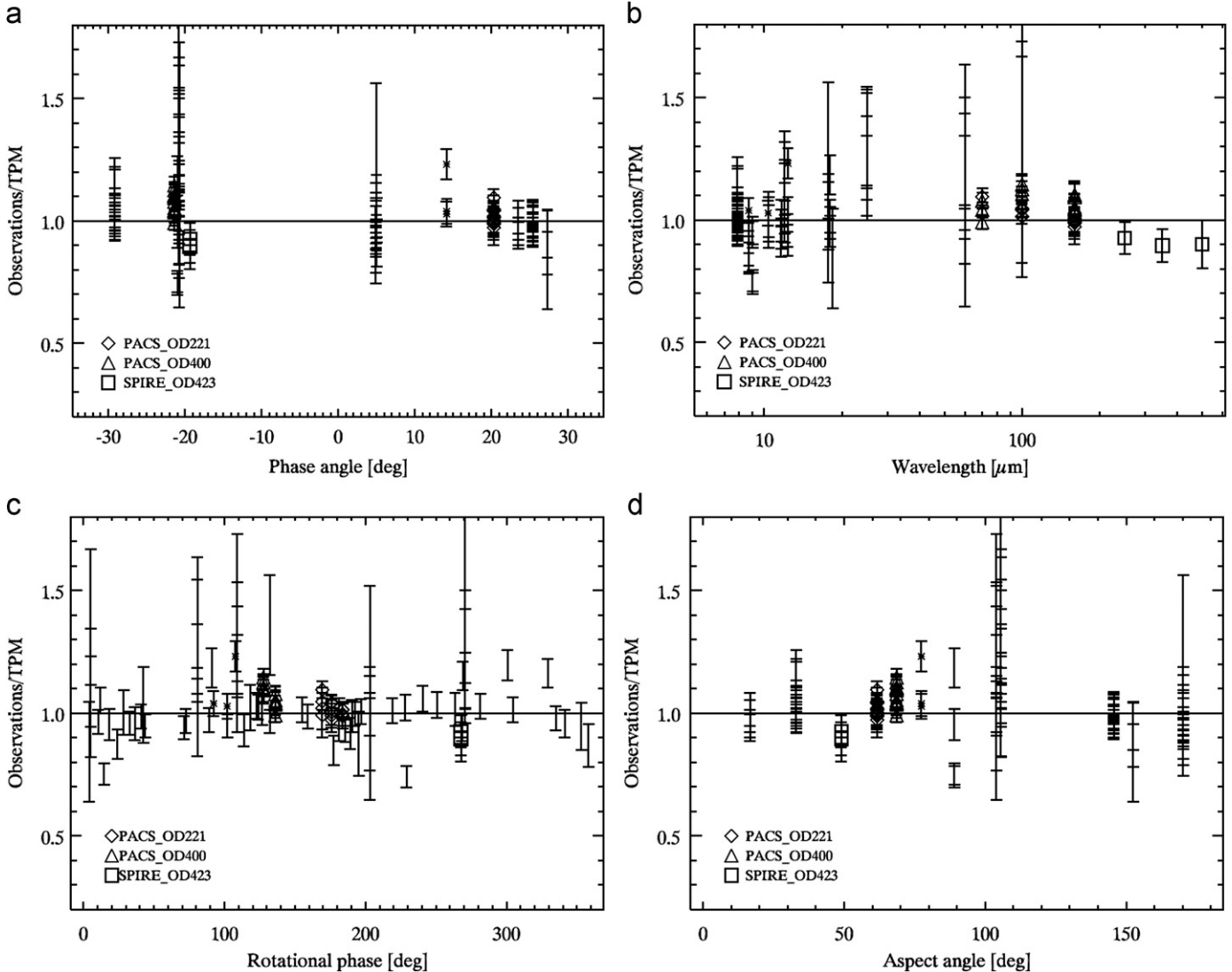


**Fig. 3.** These graphs show the wide range of observations being fit against the model where the roughness is  $\rho=0.6$  and  $f=0.7$ , and the thermal inertia was  $5 \text{ J m}^{-2} \text{ s}^{-0.5} \text{ K}^{-1}$ . The graphs show Observations/Thermal model versus (a) phase angle (b) wavelength (c) rotation phase and (d) aspect Angle.

level of roughness in combination with the LAM shape model showed that using a considerably high roughness of  $\rho=0.6$  and  $f=0.7$  we could obtain a low  $\chi^2$  value for thermal inertias below  $10 \text{ J m}^{-2} \text{ s}^{-0.5} \text{ K}^{-1}$  (SI) (See Fig. 2) with best fit found for a thermal inertia of 5 SI.

The observed fluxes of the large data set showed exceptionally high correlation with the model using this low thermal inertia and high roughness (observation/TPM versus wavelength and rotational phase — Fig. 3). This thermal inertia value of 5 SI is in agreement with (Carvano et al., 2008). It also matches with the ranges from 0–30/50 presented in Lamy et al. (2010) and Mueller et al. (2006) and also that derived from the MIRO measurements (Gulkis et al., 2012). (< 20 SI) & VIRTIS measurements (Coradini et al., 2011) (20–30 SI), but at the very low end of the scale (see Table 1). Higher thermal inertias (> 10 SI) were found to lead to much greater scattering of the data set.

Where zero roughness was applied, the analysis from the shape model also pointed to thermal inertias below 15 SI but the resulting  $\chi^2$ -values were significantly higher, indicating that the match to the observed fluxes was very weak. Indeed, some of the observations were found to be off by up to 40% from the corresponding model predictions. Another reason for excluding a smooth surface was that the best  $\chi^2$  thermal inertia range for an assumed perfectly smooth surface required an effective Lutetia size of well above 110 km (combined with a geometric albedo of about  $0.20 \pm 0.01$ ) which was clearly out of range of the actual measured values and shape model.

As a result of the above work, we conclude that Lutetia's surface must have a significant amount of small scale roughness e.g., micro-craters, to correlate with the measured thermal flux values we have obtained, a global statement for the level of roughness of (21) Lutetia which is not possible to be observed in the flyby images from Rosetta.

While our derived value for the thermal inertia is significantly smaller than the thermal inertia of the Moon it is consistent with derived values for large main-belt asteroids (Spencer and Lebofsky, 1986, 1989; Müller and Lagerros, 1998, 2002, Delbo et al., 2009). Such low thermal inertia is generally interpreted as evidence for a well-developed regolith layer with a low thermal conductivity, which might be indicative of high surface micro-porosity. Further to this, it was speculated (Spencer and Lebofsky, 1986, 1989; Müller and Lagerros, 1998, 2002) that large main-belt asteroids (> 100 km diameter) with reasonable albedos  $0.05 < pV < 0.2$  are all covered by a very low conductivity (consequently low thermal inertia) dust regolith. We therefore conclude that physical regolith properties are indeed the driving constraints for thermal emission rather than its chemical/mineralogical composition for asteroids with diameter greater than 90 km.

In addition we find, through use of the TPM and comparing our Lutetia results with those of other taxonomic types (Müller and Lagerros, 1998, 2002), that different surface materials/minerals do not influence the thermal emission significantly at least not in our broad-band far-IR measurements. The thermal behaviour is dominated instead by the regolith properties: porosity, density, conductivity, heat capacity i.e., by a low thermal inertia

## 5. Adaptation of the shape model of the side of (21) Lutetia not observed by Rosetta

Having concluded on the albedo, the H-mag value, the surface roughness, the thermal inertia and indeed the overall impact of this low thermal inertia on the regolith properties, our investigations proceeded to determine the accuracy of the LAM shape model versus the actual highly calibrated measurements obtained

by Herschel as well as other observatory data used in this current paper.

Comparison of predicted versus measured fluxes have found that, across all wavelengths in use here, the model showed a highly accurate match for the majority of the observations in question, including those provided by the two Herschel instruments. However significant deviations (10–20%) were found for the first of the two Spitzer lightcurves in use for this paper (taken at aspect angle  $33^\circ$ ) for rotational phases  $240^\circ$ – $360^\circ$ .

The corresponding Akari data at aspect angle of  $16.6^\circ$  were taken at similar rotational phases ( $190^\circ$ – $341^\circ$ ). However, while the Akari data has been found to match the model this Spitzer data set deviates in that the flux from the TPM is up to 20% less than actually measured at this area (Fig. 4). This has allowed us to pin down the shape deviations from the Spitzer case to surface areas which are only seen in the aspect angle range  $110^\circ$ – $160^\circ$  for rotational phases  $240^\circ$ – $360^\circ$  — areas not observed by Rosetta and for which the LAM shape model has a 5% error.

Fig. 5 shows the TPM output of the asteroid for the Spitzer observation. In the image, we mark where the OSIRIS data (Jorda

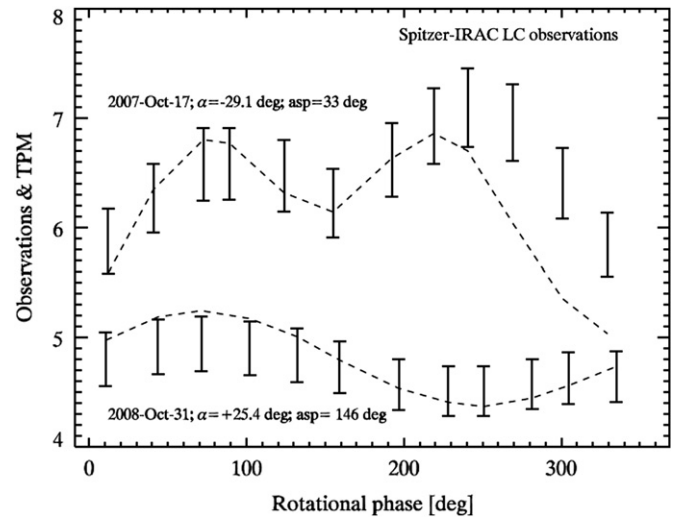


Fig. 4. Spitzer IRAC data plotted over the rotational phases. Note the mismatch of the dataset with the rotational phase beyond  $240^\circ$  corresponding to the 2007-Oct-17 observations.

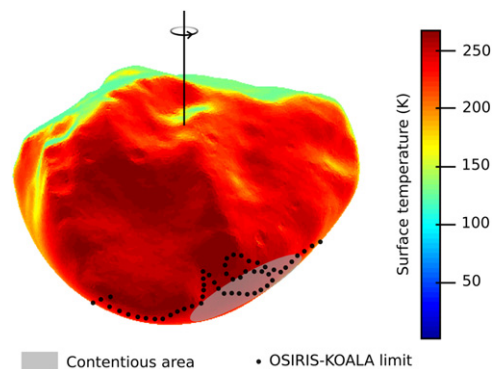


Fig. 5. Spitzer IRAS observation 2007-Oct-17 as output from the TPM. In the image, we mark where the OSIRIS data and the pre-flyby KOALA model merge (dotted-line limits shown are indicative, see Carry et al., 2012) and in particular we flag (in grey) where the contentious area is located. Based upon the fact that the grey area is visible in the thermally warmest region of the Spitzer observation, we conclude that this area would in fact require a plateau/hill or crater with a significant slope to provide the missing flux for Spitzer and to explain the discrepancy between the observed and the model flux (hot contentious area is contributing significantly to the disc-integrated flux).

et al., 2010, 2011) and the pre-flyby model (KOALA model — Carry et al., 2010; Drummand et al., 2009) merge and in particular we flag where the contentious area is located.

Based upon the fact that the area is visible in the thermally warmest region of the Spitzer observation, we conclude that, as the Spitzer fluxes are dominated by the hottest temperatures on Lutetia, the area projected by the LAM model would require a plateau/hill or crater with a significant slope to provide the increased flux for Spitzer, and to explain the discrepancy between the observed and the model flux (hot contentious area is contributing significantly to the disc-integrated flux). Our calculations show that an increase of 5 K in the contentious area would cause a 16% increase in flux at 8  $\mu\text{m}$ .

On the basis that OSIRIS saw only 60% of the surface of Lutetia, it is significant to flag how remote observations are capable of providing important inputs to allow adaptation of the shape model of that unseen area. In summary, combining measurements from both remote and in situ observations not only improves thermal property extraction and providing estimates of the surface roughness, it also can help in the identification of important alterations to the shape model of the unseen side of the asteroid.

## 6. Conclusions

In conclusion, Herschel measurements from L2 taken of (21) Lutetia around the time of the Rosetta flyby, combined with measurements from many ground based observatories allow us to conclude that this asteroid has an extremely low thermal inertia, significant small scale roughness and features on the southern hemisphere not observed by Rosetta but which can be fed into an update of the flyby model

While the in-situ measurements do indeed provide the “ground truth” for the asteroid, we believe that we have demonstrated that it is only through the performance of a joint observation campaign of an object from both remote and in-situ based spacecraft that these properties can be “finalised”. Such an approach can provide confidence not only in the accuracy of such previous pre-flyby measurements but also confidence in the techniques used in deriving those results, especially where no possibility exists for a flyby opportunity.

With this project we know now that using significant small scale roughness and low thermal inertia (combined with shape models derived from remote sensing) we can obtain “highly reliable” size and albedo information via radiometric techniques. In fact, as thermal data is (or will soon be) available for many thousand of asteroids (IRAS, MSX, ISO, Akari, Spitzer, WISE, ground-based mid-IR/submm/mm programmes, ... ), the results from (21) Lutetia can be considered to be the key to allow us to transfer our model techniques to many other targets which will not be visited by spacecraft in the near future but for which similar important questions can now be answered.

## References

Barucci, M.A., et al., 2008. Asteroids 2867 Steins and 21 Lutetia: surface composition from far infrared observations with the Spitzer space telescope. *Astronomy and Astrophysics* 477, 665–670.

Belskaya, I.N., et al., 2010. Puzzling asteroid 21 Lutetia: our knowledge prior to the Rosetta flyby. *Astronomy and Astrophysics* 515. id.A29.

Bowell, E., 1988. Application of photometric models to asteroids, Asteroids II; Proceedings of the Conference, Tucson, AZ, Mar. 8–11, 1988 (A90-27001 10-91), University of Arizona Press, 1989, pp. 524–556.

Carry, B., et al., 2010. Physical properties of the ESA Rosetta target asteroid (21) Lutetia. II. Shape and flyby geometry. *Astronomy and Astrophysics* 523, A94.

Carry, B., et al., 2012. Shape modeling technique KOALA validated by ESA Rosetta at (21) Lutetia *Planetary and Space Science* 66, 200–212.

Carvano, J.M., et al., 2008. Surface properties of Rosetta's targets (21) Lutetia and (2867) Steins from ESO observations. *Astronomy and Astrophysics* 479, 241–248.

Coradini, A., Capaccioni, F., Erard, S., Arnold, G., De Sanctis, M.C., Filacchione, G., Tosi, F., Barucci, M.A., Capria, M.T., Ammannito, E., Grassi, D., Piccioni, G., Giuppi, S., Bellucci, G., Benkhoff, J., Bibring, J.-P., Blanco, A., Blecka, M., Bockelée-Morvan, D., Carraro, F., Carlson, R., Carsenty, U., Cerroni, P., Colangeli, L., Combes, M., Combi, M., Crovisier, J., Drossart, P., Encrenaz, E.T., Federico, C., Fink, U., Fonti, S., Giacomini, S., Ip, W.H., Jaumann, R., Kürth, E., Langevin, Y., Magni, G., McCord, T.B., Mennella, V., Mottola, S., Neukum, G., Orofino, V., Palumbo, P., Schade, U., Schmitt, B., Taylor, F., Tiphene, D., Tozzi, G., 2011. The surface composition and temperature of asteroid 21 Lutetia as observed by ROSETTA/VIRTIS Science 334, 492. Available at: <<http://dx.doi.org/10.1126/science.1204062>>.

Delbo, M., et al., 2009. Thermal inertia of main belt asteroids smaller than 100 km from IRAS data. *PSS* 57 (2), 259–265.

Drummand et al., 2009. The triaxial ellipsoid dimensions, rotational pole, and bulk density of ESA Rosetta target asteroid (21) Lutetia, American Astronomical Society, DPS meeting #41, #59.07.

Fazio, G.G., 2004. The Infrared Array Camera (IRAC) for the Spitzer Space Telescope. *Astrophysical Journal Supplement Series* 154 (1), 10–17.

Griffin, M.J., et al., 2010. The Herschel-SPIRE instrument and its in-flight performance. *Astronomy and Astrophysics* 518. id.L3.

Gulkis, S., et al., 2012. Continuum and spectroscopic observations of asteroid (21) Lutetia at millimeter and submillimeter wavelengths with the MIRO instrument on the Rosetta spacecraft. *Planetary and Space Science* 66, 31–42.

Jorda, L. et al., 2010. Shape and physical properties of asteroid 21 Lutetia from OSIRIS Images, DPS meeting #42, #43.03; BAAS 42, 1043.

Jorda, L. et al., 2011. The shape and physical properties of asteroid 21 Lutetia from OSIRIS images, EGU General Assembly 2011, Geophysical Research Abstracts 13.

Lagare, P.O., Pel, J.W., et al., 2004. Successful commissioning of VISIR: the mid-infrared VLT instrument. *The Messenger* 117, 12–16.

Lagerros, J.S.V., 1996. Thermal physics of asteroids. I. Effects of shape, heat conduction and beaming. *Astronomy and Astrophysics* 310, 1011–1020.

Lagerros, J.S.V., 1997. Thermal physics of asteroids. III. Irregular shapes and albedo variations. *Astronomy and Astrophysics* 325, 1226–1236.

Lagerros, J.S.V., 1998. Thermal physics of asteroids. IV. Thermal infrared beaming. *Astronomy and Astrophysics* 332, 1123–1132.

Lamy, P.L., et al., 2010. Thermal properties of asteroid 21 Lutetia from Spitzer Space Telescope observations. *Astronomy and Astrophysics* 516. id.A74.

Mueller, M., et al., 2006. The size and albedo of Rosetta flyby target 21 Lutetia from new IRTF measurements and thermal modelling. *Astronomy and Astrophysics* 447, 1153–1158.

Müller, T., Durech, J. et al., 2011. Thermo-physical properties of 162173 (1999 JU3), a potential flyby and rendezvous target for interplanetary missions. *Astronomy and Astrophysics* 525, A145.

Müller, T., Lagerros, J.S.V., 1998. Asteroids as IR Standards for ISOPHOT. *Astronomy and Astrophysics* 338, 340–352.

Müller, T., Lagerros, J.S.V., 2002. Asteroids as calibration standards in the thermal infrared for space observatories. *Astronomy and Astrophysics* 381, 324–339.

Müller, T., et al., 2005. Thermal infrared observations of the Hayabusa spacecraft target asteroid 25143 Itokawa. *Astronomy and Astrophysics* 443, 347–355.

Ott, S. 2009. Herschel interactive processing environment, HIPE, Proceedings of the Astronomical Data Analysis Software and Systems XIX Conference, vol. 434, 139–142.

Pilbratt, G., et al., 2010. Herschel space observatory. An ESA facility for far-infrared and submillimetre astronomy. *Astronomy and Astrophysics* 518. id.L1.

Poglitsch, A., et al., 2010. The Photodetector Array Camera and Spectrometer (PACS) on the Herschel Space Observatory. *Astronomy and Astrophysics* 518. id.L2.

Sierks, H., Lamy, P., Barbieri, C., Koschny, D., Rickman, H., Rodrigo, R., A'Hearn, M., Angrilli, F., Barucci, M.A., 2011. Images of asteroid (21) Lutetia: a remnant planetesimal from the early solar system. *Science* 334, 487–490.

Spencer, L.A., Lebofsky, J.R., 1986. Asteroids II; Proceedings of the Conference, Tucson, AZ, Mar. 8–11, 1988 (A90-27001 10-91). University of Arizona Press, 1989, pp. 128–147.

Spencer, L.A., Lebofsky, J.R., 1989. Systematic biases in radiometric diameter determinations. *Icarus* 78, 337–354.

Tedesco, E.F. 1992, The IRAS Minor Planet Survey. Tech. Rpt.PL-TR-92-2049, Phillips Laboratory, Hanscom Air Force Base, Massachusetts.

Tedesco, E.F., et al., 2001MIMPS, American Astronomical Society, DPS Meeting #33, #41.24; Bulletin of the American Astronomical Society, 33, 1120.

Tedesco, E.F., et al., 2002. The supplemental IRAS minor planet survey. *The Astronomical Journal* 123, 1056–1085.

Usui, F., et al., AMAS, the AKARI/IRC mid-infrared asteroid survey, Publications of the Astronomical Society of the Pacific (PASP), submitted for publication. Available at: <<http://adsabs.harvard.edu/abs/2011arXiv1106.1948U>>2011arXiv1106.1948U>.

Werner, M.W., 2004. The Spitzer Space Telescope Mission. *Astrophysical Journal Supplement Series* 154 (1), 1–9.

Zellner, B., Gradie, J., 1976. Minor planets and related objects XX – Polarimetric evidence for the albedos and compositions of 94 asteroids. *Astronomical Journal* 81, 262–280.